Molecular Dissection of the Folding Mechanism of the α Subunit of Tryptophan Synthase: An Amino-Terminal Autonomous Folding Unit Controls Several Rate-Limiting Steps in the Folding of a Single Domain Protein†

Jill A. Zitzewitz and C. Robert Matthews*

Department of Chemistry, Life Sciences Consortium, and Center for Biomolecular Structure and Function, The Pennsylvania State University, University Park, Pennsylvania 16802

Received April 20, 1999; Revised Manuscript Received June 4, 1999

ABSTRACT: The α subunit of tryptophan synthase (αTS) from *Escherichia coli* is a 268-residue 8-stranded β/α barrel protein. Two autonomous folding units, comprising the first six strands (residues 1−188) and the last two strands (residues 189−268), have been previously identified in this single structural domain protein by tryptic digestion [Higgins, W., Fairwell, T., and Miles, E. W. (1979) *Biochemistry 18*, 4827−4835]. The larger, amino-terminal fragment, αTS(1−188), was overexpressed and independently purified, and its equilibrium and kinetic folding properties were studied by absorbance, fluorescence, and near- and far-UV circular dichroism spectroscopies. The native state of the fragment unfolds cooperatively in an apparent two-state transition with a stability of 3.98 ± 0.19 kcal mol^{-1} in the absence of denaturant and a corresponding *m* value of 1.07 ± 0.05 kcal mol^{-1} M^{-1}. Similar to the full-length protein, the unfolding of the fragment shows two kinetic phases which arise from the presence of two discrete native state populations. Additionally, the fragment exhibits a significant burst phase in unfolding, indicating that a fraction of the folded state ensemble under native conditions has properties similar to those of the equilibrium intermediate populated at 3 M urea in full-length αTS. Refolding of αTS(1−188) is also complex, exhibiting two detectable kinetic phases and a burst phase that is complete within 5 ms. The two slowest isomerization phases observed in the refolding of the full-length protein are absent in the fragment, suggesting that these phases reflect contributions from the carboxy-terminal segment. The folding mechanism of αTS(1−188) appears to be a simplified version of the mechanism for the full-length protein [Bilsel, O., Zitzewitz, J. A., Bowers, K.E, and Matthews, C. R.(1999) *Biochemistry 38*, 1018−1029]. Four parallel channels in the full-length protein are reduced to a pair of channels that most likely reflect a cis/trans proline isomerization reaction in the amino-terminal fragment. The off- and on-pathway intermediates that exist for both full-length αTS and αTS(1−188) may reflect the preponderance of local interactions in the β/α barrel motif.

Protein fragments that are capable of folding in the absence of the remainder of the polypeptide have the potential to provide valuable insights into the mechanism of folding of the full-length protein from which they are derived. Autonomously folding fragments may serve to arrest folding at various points along the folding pathway, potentially providing stable models for transient intermediates whose short lifetimes make them difficult to study (*1, 2*). Kinetic studies of fragments, when compared to the often complex behavior of the full-length protein, may yield information about the regions of the protein that are responsible for the observed rate-limiting steps in the folding of the full-length protein.

A common problem with the fragmentation approach, however, is the identification of segments that are capable of autonomously folding. Highly cooperative equilibrium folding reactions often imply that partial sequences cannot adopt a stable fold. For example, fragments of barnase (*3*), chymotrypsin inhibitor-2 (*4*), and thioredoxin (*5*) do not fold significantly in isolation although fragment complementation studies in these systems have yielded valuable insights into the folding mechanism of the corresponding full-length proteins (*6*).

One potential solution to this problem for large proteins is to examine the behavior of proteolytically derived or engineered fragments that contain more than ∼100 residues. For example, a 101-residue fragment of the β_2 subunit of tryptophan synthase folds in less than a few milliseconds to an ensemble of conformations with significant secondary structure, providing a stable model for an early folding intermediate (*7*). The amino-terminal 107 residues and the carboxy-terminal 123 residues of dihydrofolate reductase can fold to marginally stable forms that span 2 structural domains (*8*). The autonomous folding of these fragments may be related to the existence of parallel folding channels (*9*). Two protein engineered fragments corresponding to the amino- and carboxy-terminal structural domains of yeast phosphoglycerate kinase both exhibited complex multiphasic refold-

† This work was supported by the National Institutes of Health through grant GM23303 to C.R.M. Partial support was also provided by NIH Postdoctoral Fellowship Award GM14954 to J.A.Z.

* To whom correspondence should be addressed. Phone: (814) 865-8859. FAX: (814) 863-8403. Email: crm@psu.edu.

10.1021/bi9909041 CCC: $18.00
Published on Web 07/13/1999

ing kinetics although they do not associate (*10*). These results as well as complementation studies on fragments larger than a single structural domain (*11*) suggest that folding and domain pairing in the full-length protein are simultaneous events.

An alternative solution for multisubunit proteins is to create fragments that define the interface between the subunits. The mutual stabilization gained by spontaneous association of a pair of 65-residue core fragments of dimeric tryptophan repressor yields a simplified, single channel, folding mechanism that retains the essential features of the three parallel channel mechanism of the full-length protein (*12*). These features include a nearly diffusion-limited reaction that produces a transient, dimeric intermediate whose conversion to native is the rate-limiting step in folding (*13*). A 435-residue fragment corresponding to the isolated β helix domain of p22 tailspike protein associates to form a stable nativelike trimer which unfolds reversibly in urea (*14*). This trimeric fragment provides a useful model for studying the folding of the corresponding full-length protein because it unfolds with comparable kinetics but is not plagued by aggregation problems common in the full-length system (*15*).

The 268-residue, 8-stranded β/α barrel protein, α subunit of tryptophan synthase (αTS),[1] provides an example of a monomeric, single structural domain protein that is amenable to fragmentation studies. Tryptic digestion of the tryptophan synthase $\alpha_2\beta_2$ holoenzyme (*16*) has previously identified an 188-residue amino-terminal fragment of αTS which unfolds cooperatively in Gdn-HCl (*17*). This fragment was originally considered to be a model for the equilibrium intermediate of αTS, termed I1, that is populated in the presence of moderate concentrations of denaturant (*17, 18*). More recent results based on mutagenic (*19*), calorimetric (*20*), and time-resolved anisotropy (*21*) studies have demonstrated that the carboxy-terminal residues also participate in I1. A second equilibrium intermediate that is populated at high concentrations of denaturant, termed I2, has been identified by ^{1}H NMR, circular dichroism, and fluorescence spectroscopy (*22, 23*). A related, although somewhat destabilized, stable form exists in a set of amino-terminal fragments of αTS containing at least the first four $\beta\alpha$ units, i.e., residues 1−147 (*24*).

The kinetics of folding of αTS in urea (*25*−*27*) and Gdn-HCl (*28, 29*) have also been well characterized. A mechanism has recently been proposed based on the results of a global analysis of stopped-flow and manual-mixing circular dichroism kinetic refolding and unfolding data (*30*). The protein folds through multiple parallel channels each with multiple native, intermediate, and unfolded forms. In addition, an off-pathway intermediate is populated within 5 ms that subsequently unfolds to produce a set of I1-like, on-pathway intermediates.

In an effort to further understand the role that the first six β strands of αTS play in the formation of both equilibrium and kinetic folding intermediates, the folding of αTS(1−188) from urea has been characterized by circular dichroism, absorbance, and fluorescence spectroscopies. The results highlight a key role for the amino-terminal 188 residues in controlling the folding of αTS.

MATERIALS AND METHODS

Reagents. Oligonucleotides used for mutagenesis were obtained from the Midland Certified Reagent Co. (Midland, TX). Ultrapure urea was purchased from ICN Biomedicals, Inc. (Costa Mesa, CA), and used without further purification in most cases. For some unfolding experiments, the urea was further recrystallized from water to remove impurities that absorb in the far-UV. ANS was purchased from Molecular Probes (Eugene, OR). All other chemicals were reagent grade.

Protein Expression and Purification. Full-length αTS was expressed and purified as described previously (*30*). The amino-terminal fragment was expressed as inclusion bodies in the CB149 *Escherichia coli* strain containing the plasmid pXH(1−188). The construction of pXH(1−188), which contains a double stop codon in the gene for αTS after Arg188, has been described previously (*24*). A modified version of the protocol of Tsuji et al. was used to recover the insoluble fragment (*19*). Briefly, the cells were suspended in 100 mM potassium phosphate, pH 7.8, 5 mM K_2EDTA, and 2 mM DTE and lysed by sonication. After centrifugation at 45000*g* for 45 min at 4 °C to remove the soluble protein fraction, the insoluble protein pellet was unfolded in 6 M urea with stirring at 4 °C. After centrifugation at 45000*g* for 1 h at 4 °C, the amino-terminal fragment, which remained in the supernatant, was refolded by dropwise addition into a 10-fold excess of buffer.

All purification steps were carried out at 4 °C in buffer containing 10 mM potassium phosphate, pH 7.8, 2 mM K_2-EDTA, and 1 mM DTE. αTS(1−188) first was purified by ion-exchange chromatography on a DEAE column using an exponential gradient from 0 to 300 mM KCl. Alternatively, the fragment was purified by hydrophobic chromatography on a butyl Sepharose column (Pharmacia, Piscataway, NJ). The fragment and column were preequilibrated in 0.4 M ammonium sulfate prior to loading the protein onto the column. The protein was eluted by a linear dilution of the ammonium sulfate concentration. Both methods required a second purification step on a G-100 Superose sizing column (Pharmacia).

Protein purity was >95%, as determined by the presence of a single band on a 15% sodium dodecyl sulfate−polyacrylamide gel. The molecular mass, measured by electrospray mass spectrometry, was within 0.1% of the calculated mass. Protein concentrations for αTS(1−188) were determined from the tyrosine absorbance at 277 nm, using an extinction coefficient of 9067 M^{-1} cm^{-1} (*31*). The protein was stored in 80−90% saturated ammonium sulfate solutions and dialyzed just before use against standard buffer used for all folding experiments: 10 mM potassium phosphate, pH 7.8, 0.2 mM K_2EDTA, and 1 mM β-mercaptoethanol.

Equilibrium Ultracentrifugation. Equilibrium ultracentrifugation data were collected on a Beckman XL-I analytical

[1] Abbreviations: AB, absorbance; ANS, 1-anilino-8-naphthalenesulfonate; αTS, α subunit of tryptophan synthase from *Escherichia coli*; αTS(1−188), residues 1−188 of the α subunit of tryptophan synthase from *Escherichia coli*; BME, β-mercaptoethanol; CD, circular dichroism; CMW, center-of-mass wavelength; DTE, dithioerythritol; F, folded state of αTS(1−188); FL, fluorescence; FPLC, fast performance liquid chromatography; Gdn-HCl, guanidine hydrochloride; I1, equilibrium folding intermediate of αTS populated in ~3 M urea; I2, equilibrium folding intermediate of αTS populated in ~5 M urea; K_2EDTA, ethylenediaminetetraacetic acid, dipotassium salt; N, native state of αTS; PCR, polymerase chain reaction; SF, stopped-flow; U, unfolded state.

ultracentrifuge. Absorbance as a function of radial distance was collected at 230, 280, and 290 nm for initial protein concentrations of 10, 50, and 100 μM, respectively, using an eight-cell rotor rated at 50 000 rpm. Equilibrium sedimentation experiments were run at 35 000 rpm for >36 h until equilibration was reached. Data were analyzed using previously described methods (*32*).

Equilibrium Unfolding Experiments. To characterize the equilibrium properties, αTS(1−188) was equilibrated by manual methods with incremental amounts of ultrapure urea in folding buffer at 25 °C. Samples were maintained at 25 °C for ≥1 h to ensure complete equilibration prior to data collection. Circular dichroism spectra were collected on an Aviv Model 62DS CD spectrophotometer equipped with a thermoelectric cell holder. Far-UV CD data were collected from 200 to 300 nm using a 2 mm cell path length and a 2 s averaging time. Near-UV CD spectra were collected from 250 to 320 nm using a water-jacketed 10 cm cell. To improve the signal-to-noise ratio, 5 spectra were averaged at each urea concentration. Absorbance data were acquired on an AVIV refurbished CARY 118DS spectrometer. Total intensity fluorescence spectra were collected on a Spex Fluorolog 2 from 295 to 450 nm using an excitation wavelength of 277 nm and excitation and detection bandwidths of 3.7 nm. Anisotropy data were collected on an Aviv Model ATF105 spectrofluorometer with Glan-Taylor polarizers and analyzed as described previously (*32*). Samples were excited at 278 nm, and the emission was detected at 308 nm. A Hamilton 540B automatic titrator was utilized to perform the titration using stocks of αTS(1−188) in buffer and in approximately 9 M urea; the exact urea concentration of the unfolded stock was determined by measuring the refractive index (*33*). Equilibration times between additions were sufficient to observe no further change in signal, ∼300−1000 s. A detailed description of the approach has been reported previously (*34*).

Kinetic Unfolding and Refolding Experiments. CD and fluorescence manual mixing experiments were performed on an Aviv Model 62DS or 62ADS CD spectrophotometer or an Aviv Model ATF105 spectrofluorometer, respectively, all equipped with an Aviv thermoelectric cell holder. These experiments were performed using a 1 cm cell path length and an averaging time of 1 s. The dead-time for manual mixing experiments was ∼4 s, although an additional 6 s of data were omitted to account for the instrument response time. Unfolding jumps were performed from 0 M urea to various final concentrations of urea (1.8−8 M). Unfolding jumps from various initial concentrations (0−5.2 M) to a final concentration of 5.5 M urea were also carried out. Refolding jumps were performed from 6 M to various final concentrations of urea (0.6−3.5 M).

Stopped-flow CD experiments were performed on an Aviv Model 62DS CD spectrophotometer with an attached Bio-logic SFM-3 stopped-flow drive train or with an AVIV Model 202SF stopped-flow CD spectrometer. Stopped-flow tyrosine and ANS fluorescence experiments were performed on a Bio-logic SFM-3 stopped-flow spectrofluorometer equipped with a Bio-Logic modular light source and monochromator. For tyrosine fluorescence experiments, total emission intensities were collected upon excitation at 278 nm with a 5 nm bandwidth. For the ANS fluorescence experiments, samples were excited at 370 nm, and the emission above 460 nm was collected using a cutoff filter supplied by Durrum. ANS stock solution concentrations were determined by measuring the absorbance at 370 nm using a molar extinction coefficient of 6800 M^{-1} cm^{-1}. For all stopped-flow experiments, the temperature of the syringe reservoirs and mixing chamber was maintained at 25 °C using an attached water bath or a thermoelectically controlled housing. The cell path length was 1.0, 1.5, or 2.0 mm. The dead-time for both refolding and unfolding was estimated to be 5 ms (*35*).

Equilibrium and Kinetic Data Analysis. Equilibrium unfolding data were fit to the apparent two-state model, F ⇄ U, where F and U represent the folded and unfolded forms, respectively. The apparent free energy of unfolding in the absence of urea, $\Delta G°(H_2O)$, was obtained by assuming a linear dependence of the free energy of unfolding on the denaturant concentration, $\Delta G° = \Delta G°(H_2O) + m[\text{urea}]$ (*36*).

Individual kinetic traces were fit to a sum of exponentials:

$$A(t) = A(\infty) + \sum A_i e^{-t/\tau_i}$$

where *A(t)* and *A*(∞) are the total amplitude at time *t* and the amplitude at infinite time, respectively. A_i and τ_i are the amplitude and the time constant for the *i*th component of the fit. All equilibrium and kinetic data were fit using Savuka, version 5.12, an in-house nonlinear least-squares program (*30, 37*).

RESULTS

A variety of spectroscopic techniques can be used to probe both the equilibrium and kinetic folding properties of αTS-(1−188). Equilibrium CD experiments have previously demonstrated significant, cooperatively folded, secondary structure in αTS(1−188) (*16, 17, 24*). The tertiary structure can be probed by monitoring the environment of the tyrosine side chains by absorbance, fluorescence, and near-UV CD spectroscopies; *Escherichia coli* αTS does not contain tryptophan. Six of the seven tyrosine residues in the full-length protein are contained in the amino-terminal fragment (Figure 1), providing useful probes for both equilibrium and kinetic experiments on the folding of αTS(1−188).

Equilibrium Ultracentrifugation Studies. Previous FPLC size-exclusion chromatography studies have demonstrated that αTS(1−188) has some tendency to dimerize in the absence of urea, presumably because the removal of two β strands from the C-terminus of αTS exposes hydrophobic surface (*24*). Equilibrium ultracentrifugation studies were performed to quantify the extent of dimerization. The data were best described by a simple monomer-to-dimer equilibrium (data not shown), yielding a dissociation constant of $(2.4 \pm 0.3) \times 10^{-4}$ M. To minimize the effects of dimerization on the equilibrium and kinetic folding properties of αTS(1−188), the concentration of fragment was maintained at less than 20 μM for all folding studies. For most studies, the concentration was held constant at ∼5 μM, where the percent dimer is estimated to be ∼2%.

Spectral Properties. The far-UV CD spectrum of αTS-(1−188) (*24*), like that of full-length αTS, displays a minimum at 220 nm and a maximum at 193 nm, indicative of a mixed α/β structure (data not shown). The fragment exhibits significant secondary structure; however, the mean residue ellipticities of αTS(1−188) at 193 and 220 nm (19.0

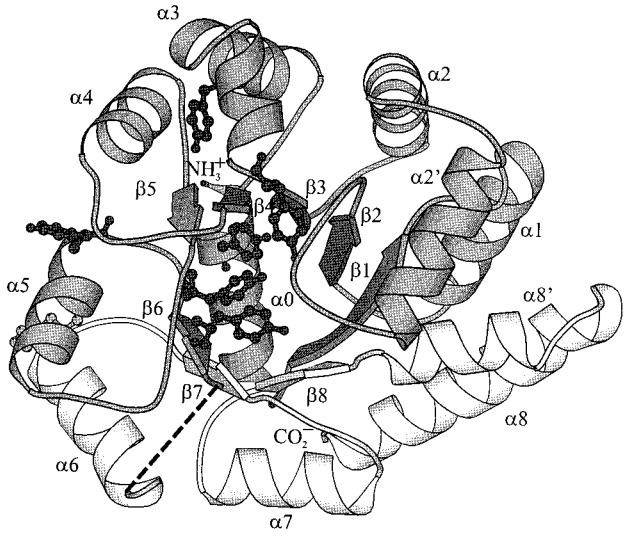

FIGURE 1: Ribbon diagram of αTS from *Salmonella typhimurium* (*53*) generated with Molscript version 2.0.2 (*54*). Sequence identity at 228 of the 268 residues and the ability of αTS from *E. coli* and S. *typhimurium* to activate the β_2 subunits from both strains (*55*) support the assumption that the two structures are very similar. The secondary structural elements corresponding to αTS(1−188) are shown in dark gray, and those for αTS(189−268) are shown in light gray. Side chains for the seven tyrosine residues are shown, and the dashed line represents missing coordinates for a disordered loop encompassing residues 178−189.

and −13.3 mdeg cm^2 dmol^{-1}, respectively) are decreased relative to full-length αTS (31.4 and −16.1 mdeg cm^2 dmol^{-1}, respectively), indicating that the fragment has less structure on a per residue basis. The tyrosine FL emission spectrum of αTS(1−188) is also quite similar to that of full-length αTS (*23*), exhibiting a maximum at ∼305 nm and a shoulder at ∼365 nm when exciting at 278 nm (data not shown). The fluorescence quantum yield of the 305 nm peak for the fragment is decreased relative to that for full-length αTS, reflecting either an increased solvent exposure of some of the tyrosine residues in the fragment or missing contributions from tyrosine 204.

Urea Denaturation Studies. Equilibrium unfolding experiments were performed to determine the stability of αTS(1−188) to urea denaturation. The disruption of secondary structure, probed by monitoring the far-UV CD signal at 222 nm, is shown in Figure 2A. The CD data exhibit a cooperative folding transition between 2 and 5 M urea, as well as small, linear changes in signal from 0 to 2 M urea and from 5 to 8 M urea in the native and unfolded baseline regions, respectively. A similar smooth sigmoidal unfolding transition, which showed no evidence for an equilibrium intermediate, has been observed previously by CD for the Gdn-HCl denaturation of αTS(1−188) (*17*).

The disruption of tertiary structure was probed by monitoring the absorbance at 287 nm (Figure 2A) and the fluorescence at 305 nm (Figure 2B). Both techniques also show evidence for a cooperative unfolding transition between 2 and 5 M urea. In contrast to the far-UV CD data, the FL and AB data show a more substantial urea dependence in the native baseline region between 0 and 2 M urea, indicating a significant change in the solvent exposure of the tyrosine residues in this region. When the fluorescence data are plotted as center-of-mass wavelength, CMW, as a function of urea (Figure 2B), an 8 nm red shift is observed between the folded

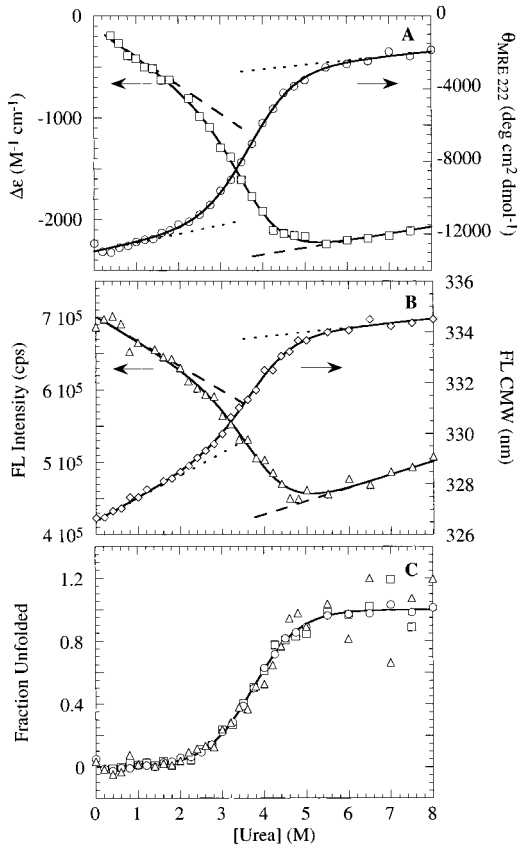

FIGURE 2: Equilibrium unfolding of αTS(1−188). (A) Dependence of the mean residue ellipticity at 222 nm (circles) and the extinction coefficient at 287 nm (squares) on the urea concentration. Protein concentration was 13.9 μM. (B) Dependence of the fluorescence intensity at 305 nm (triangles) and fluorescence CMW (diamonds) on the urea concentration. Protein concentration was 5 μM. (C) The apparent fraction of unfolded protein as a function of [urea]. Lines in panels A and B represent fits of individual data sets to an apparent two-state equilibrium unfolding model according to the method of Santoro and Bolen (*56*); the fitted baselines are indicated by dashed lines. The line in panel C represents a global fit of CD, AB, and FL intensity data shown in panels A and B to an apparent two-state model. Buffer conditions were 10 mM potassium phosphate, pH 7.8, 0.2 mM K_2EDTA, and 1 mM β-mercaptoethanol at 25 °C.

and unfolded fragments. The relatively small change in fluorescence intensity across the unfolding transition means that CMW provides an accurate measure of the thermodynamic properties (*21*).

The normalized fraction unfolded plots for the CD, AB, and FL unfolding curves are compared in Figure 2C. In these plots, the linear urea dependence observed between 0 and 2 M urea was assumed to represent the native baseline region for the fragment. The scatter observed in the AB and FL plots at high concentrations of urea is a direct result of the steep native baselines that intersect the unfolded baselines at high urea concentrations. Nonetheless, the near-coincidence of the transitions observed by all three techniques demonstrates that secondary and tertiary structures are disrupted simultaneously.

The apparent thermodynamic stability of the fragment was estimated by fitting the data to apparent two-state equilibrium unfolding transitions. Fits of individual data sets are given in Table 1. The comparable results obtained at protein concentrations ranging from 2.5 to 20 μM demonstrate that

Table 1: Apparent Thermodynamic Parameters for the Unfolding of αTS(1−188)[a]

technique	protein concn (μM)	$\Delta G°(H_2O)$ (kcal mol^{-1})	$-m$ (kcal mol^{-1} M^{-1})	C_m[b] (M)
AB at 287 nm	13.9	4.16 ± 0.44	1.12 ± 0.11	3.73
CD at 222 nm	2.5	4.08 ± 0.99	1.11 ± 0.25	3.67
	13.9	3.97 ± 0.28	1.07 ± 0.07	3.72
	20.0	3.96 ± 0.37	1.09 ± 0.10	3.65
FL at 305 nm	5.0	4.31 ± 0.89	1.09 ± 0.11	3.94
FL CMW	5.0	4.14 ± 0.45	1.09 ± 0.11	3.81
global[c]		3.98 ± 0.19	1.07 ± 0.05	3.73

[a] Data were fit to the apparent two-state model: F ⇄ U. [b] Errors in C_m are estimated to be ±0.15 M urea. [c] Simultaneous fit of the following three data sets: 13.9 μM AB at 287 nm, 13.9 μM CD at 222 nm, and 5 μM FL at 305 nm.

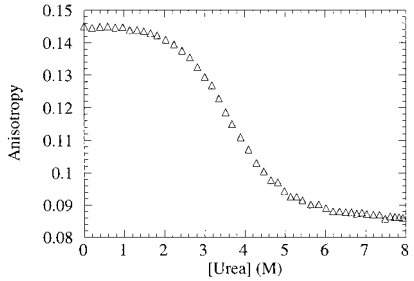

FIGURE 3: Steady-state fluorescence anisotropy at 308 nm as a function of [urea]. Protein concentration was 10 μM, and the buffer conditions are described in the caption to Figure 2.

the equilibrium unfolding process being monitored is not influenced by the slight propensity of this fragment to dimerize. A global fit of the intensities observed by CD, AB, and FL yields a free energy in the absence of denaturant under standard state conditions of 3.98 ± 0.19 kcal mol^{-1} and an m value of 1.07 ± 0.05 kcal mol^{-1} M^{-1}.

Evidence for Specific Tertiary Packing. The environment of the tyrosine residues was further probed by steady-state fluorescence anisotropy. Figure 3 shows the anisotropy of αTS(1−188) as a function of urea concentration. Although the solvent exposure of the tyrosine residues increases significantly at low concentrations of urea (Figure 2B), the rotational mobility of the tyrosines is nearly independent of urea in this same concentration range (Figure 3). The sigmoidal decrease in anisotropy above 2 M urea reflects the cooperative unfolding transition that releases the tyrosines from their well-packed environments in the folded form of αTS(1−188). Efforts to fit the vertical-vertical and vertical-horizontal fluorescence components simultaneously to either a two-state or a three-state equilibrium model (*34*) were unsuccessful, presumably as a consequence of the steep native baseline observed for the fluorescence intensity (Figure 2B).

The near-UV CD spectrum of αTS(1−188) is shown in Figure 4A. Consistent with previously reported results (*16*), the spectrum displays a broad minimum in the tyrosine region between 275 and 290 nm and two distinct minima at 264 and 271 nm in the phenylalanine region. Also shown in Figure 4A are the near-UV spectra of the full-length αTS at 0, 3, and 9 M urea, under conditions where the native, I1 intermediate, and unfolded forms, respectively, are significantly populated. The near-UV CD spectrum of 1−188 qualitatively resembles the αTS spectrum in 3 M urea,

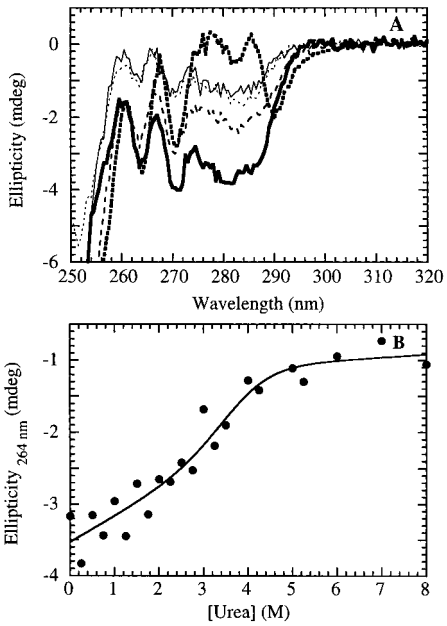

FIGURE 4: (A) Near-UV CD spectra of αTS(1−188) in 0 M urea (thick solid line) and 9 M urea (thin solid line) as well as full-length αTS in 0 M (thick dotted line), 3 M (dashed line), and 9 M urea (thin dotted line) where the N, I1, and U states, respectively, are significantly populated. (B) [Urea] dependence of the near-UV CD signal at 264 nm. Protein concentrations were 10 μM, and other conditions are described in the caption to Figure 2.

suggesting that the packing of aromatic residues in the fragment and I1 may be similar. The differences between the spectra may also reflect the absence of one tyrosine and two phenylalanines in the segment from 189 to 268. The ellipticity at 264 nm for αTS(1−188) as a function of urea is shown in Figure 4B. The ellipticity at 264 nm, as well as the ellipticity at the other peak maxima at 271 and 280 nm (data not shown), decreases gradually with increasing urea concentrations before attaining a constant value at ∼5 M urea. Although the small signal change and low signal-to-noise precluded accurate estimates of the thermodynamic stability, the apparent midpoint of the transition, ∼3.5 M urea, is consistent with the cooperative disruption of structure detected by other optical techniques (Figure 2).

Kinetic Unfolding Studies. A representative kinetic unfolding trace obtained by manual-mixing CD is shown in Figure 5A. Unlike the unfolding of full-length αTS (*30*), the total change in ellipticity for the fragment does not match the value expected from equilibrium experiments. Instead, approximately half of the signal is lost within the manual-mixing dead-time of ∼5 s, demonstrating the presence of a rapid unfolding reaction. Comparable burst phase amplitudes were obtained by stopped-flow CD experiments (data not shown), indicating that this rapid unfolding reaction occurs in less than 5 ms. The I1 intermediate observed in full-length αTS unfolds within 5 ms (*30*), suggesting that the burst phase species observed in the fragment may reflect the unfolding of an I1-like species that is populated in the absence of denaturant.

Similar to the unfolding of full-length αTS (*30*), two subsequent observable kinetic phases are present when unfolding to 5 M urea. The faster phase, τ1, has a time constant of 25 s, and the slower phase, τ2, has a time constant of ∼140 s. The amplitudes of the fast and slow phases are

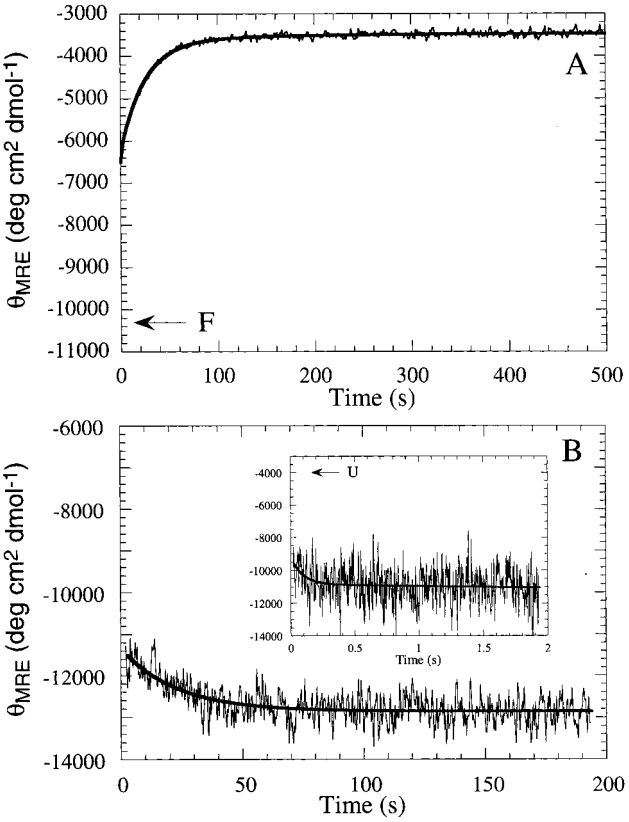

FIGURE 5: Manual-mixing unfolding (A) and stopped-flow refolding (B) kinetic traces for αTS(1−188) monitored by CD spectroscopy at 222 nm. Unfolding was initiated by a 1:10 dilution of fragment in buffer to a final concentration of 5 M urea; refolding was initiated by a 1:10 dilution of fragment in 6 M urea to a final concentration of 0.6 M urea. The initial signal expected for the folded form, F, at 5 M urea is indicated in panel A, and the initial signal expected for the unfolded form, U, in 0.6 M urea is indicated by an arrow in the inset to panel B. Smooth lines represent fits of the data to two exponentials. The final protein concentration was 5 μM, and the buffer conditions are described in the caption to Figure 2.

92% and 8%, respectively, similar to the partitioning of the amplitudes observed for the two phases in full-length αTS (*30*). Neither unfolding time constant exhibits a protein concentration dependence in the range of 1−10 μM (data not shown).

Figure 6 shows the unfolding time constants of the two observable phases as a function of final urea concentration. The unfolding time constants of the major fast and minor slow phases are slightly shorter than those for full-length αTS; however, the urea dependences are comparable. Under strongly unfolding conditions (>4 M), the amplitudes of both phases are independent of the final urea concentration (data not shown). The slow phase accounts for ∼10% and the fast phase for ∼90% of the change in signal expected from equilibrium studies (Figure 2A). Only the principal, faster phase was detected in most stopped-flow CD unfolding experiments, presumably because of the lower signal-to-noise ratio in these experiments.

Unfolding jumps from varying initial urea concentrations (0−5 M urea) to a final concentration of 5.5 M urea were performed to determine whether one of the observable unfolding phases results from the sequential unfolding of the native form through an intermediate or whether two native conformers are present. The amplitudes of both unfolding phases decrease simultaneously with a midpoint

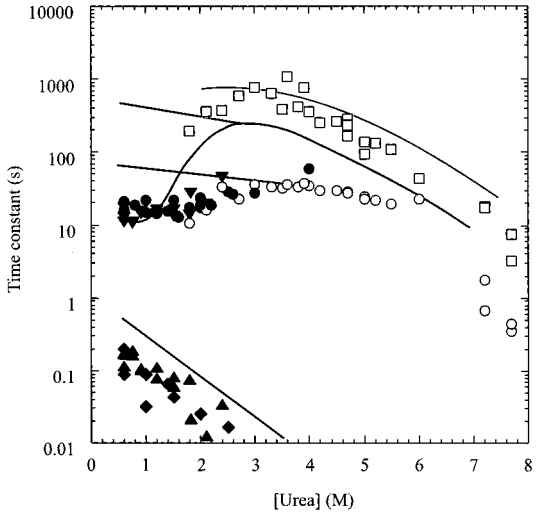

FIGURE 6: Observed time constants as a function of [urea] for refolding (closed symbols) and unfolding (open symbols) as monitored by manual-mixing and stopped-flow CD (circles, diamonds, and squares) and stopped-flow ANS FL (upright and inverted triangles). Refolding data were acquired using stopped-flow techniques, and unfolding data were acquired by manual-mixing techniques with the exception of the points at urea concentrations >6 M that were acquired by stopped-flow. Lines represent observed relaxation times for full-length αTS (*30*). Protein concentrations were 2−7 μM, ANS concentration was 200 μM, and the buffer conditions are described in the caption to Figure 2.

near the midpoint of the equilibrium unfolding reaction (data not shown), suggesting that the two unfolding reactions are not sequential but, more likely, occur in parallel. Two native conformers that unfold through parallel channels have also been observed in the unfolding of the full-length protein (*30*).

Kinetic Refolding Studies. Figure 5B shows the refolding of αTS(1−188) under strongly refolding conditions (6 → 0.6 M urea) as monitored by stopped-flow CD. Approximately 60% of the signal is acquired within the dead-time of the experiment (Figure 5B, inset), demonstrating the presence of a burst phase intermediate. The subsequent kinetic response is best fit to a sum of two exponentials having time constants of 160 ms (τ1) and 16 s (τ2). The observed amplitude is partitioned nearly equally between these two kinetic phases at all final urea concentrations (data not shown). The time constants for both observable phases were independent of fragment concentration in the range of 1−10 μM (data not shown), demonstrating that the tendency of the fragment to self-associate does not perturb the folding process. Although similar results were obtained by stopped-flow tyrosine FL (data not shown), photobleaching precluded accurate estimates of the time constants in these experiments.

The refolding time constants obtained by SF-CD as a function of final urea concentration are shown in Figure 6. Also shown are the two time constants observed for the refolding of the fragment in the presence of the hydrophobic dye ANS. ANS fluoresces strongly at 480 nm when bound to nonpolar surfaces (*38*), providing a means to monitor partially folded proteins (*39*, *40*). The similarity of the time constants observed by CD and ANS FL demonstrates that the formations of secondary structure and hydrophobic surfaces occur on a comparable time scale. The similar responses by intrinsic and extrinsic probes also imply that ANS binding does not significantly alter the folding mechanism (*41*).

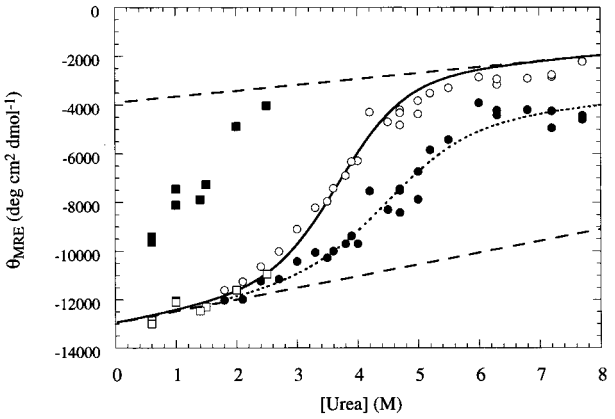

FIGURE 7: [Urea] dependence of the unfolding (circles) and refolding (squares) burst phase amplitudes of αTS(1−188) as monitored by manual-mixing and stopped-flow CD, respectively, at 222 nm. The solid line represents the two-state fit of the equilibrium data taken from Figure 2A, and the dashed lines represent the fitted baselines. Open symbols represent the final amplitudes from the kinetic experiments; reversibility is demonstrated by the coincidence of the final amplitudes measured kinetically with the equilibrium values. Conditions are described in the caption to Figure 2.

The slower refolding phase, $\tau 2$, is nearly independent of urea at low concentrations and exhibits a slight urea dependence between 2 and 4 M urea, suggesting that it reflects an isomerization or rearrangement reaction (*42*). The faster refolding phase, $\tau 1$, has a significant urea dependence and accelerates with increasing urea concentrations. The negative slope for the urea dependence of the time constant for the $\tau 1$ phase is consistent with an unfolding reaction. A similar urea dependence observed for the fastest refolding kinetic phase of the full-length protein has been attributed to the unfolding of an off-pathway burst phase species to form an I1-like intermediate (*30*).

Burst Phase Stability. The apparent stabilities of the unfolding and refolding burst phase intermediates can be determined by measuring the amplitude as a function of the final urea concentration (*13, 35, 43, 44*). The rationale for this experiment is based upon the proportionality of the signal to the concentration of the intermediate and the absence of kinetic coupling to subsequent phases which are orders of magnitude slower (*45*). The urea dependences of the burst phase species observed in the unfolding and refolding of αTS(1−188) when monitored by SF-CD are shown in Figure 7.

The monotonic decrease in the amplitude of the refolding burst phase with increasing urea concentration indicates that the burst phase species observed in refolding has only marginal stability. This response is similar to that observed for full-length αTS (*30*). The amplitude of the unfolding burst phase species decreases sigmoidally with increasing urea concentration, exhibiting a midpoint of ∼4.5 M urea. A fit of the total observed amplitude to an apparent two-state transition yields apparent free energy and *m* value estimates for the unfolding of the burst phase species of 3.96 ± 0.52 kcal mol^{-1} and 0.87 ± 0.12 kcal mol^{-1} M^{-1}, respectively. These values are comparable to free energy and *m* value measurements obtained under equilibrium conditions for the folded fragment (Table 1). Along with the biphasic unfolding reaction, the sigmoidal increase in the burst phase amplitude implies that the folded state of αTS(1−188) is composed of several distinct kinetic species.

DISCUSSION

Equilibrium Folding Properties of αTS(1−188). The equilibrium unfolding process for αTS(1−188), monitored by several optical techniques, is well described by a model involving two principal thermodynamic states, F and U. The apparent free energy of folding of this fragment, 3.98 kcal mol^{-1}, is lower than that of most globular proteins (*33*), and the dependence of the free energy on the denaturant concentration, i.e., the *m* value, 1.07 kcal mol^{-1} M^{-1}, is significantly less than would be expected for a well-folded globular protein containing 188 amino acids (*46*). The *m* value and free energy might be reduced relative to those expected for a globular protein of 188 residues because of the loss of stabilizing interactions and the increase in hydrophobic surface upon deletion of the C-terminal domain. However, the magnitude of the reduction suggests that the fragment cannot adopt a structure that is as compact as when in the context of the full-length protein. Consistent with this supposition are the results of time-resolved fluorescence anisotropy experiments on αTS(1−188), which suggest that it has a hydrodynamic radius that is ∼15% larger than expected for a globular protein of 188 residues (*21*). This conclusion is not surprising considering that the two carboxy-terminal strands are absent and that six-stranded barrels have not been observed in crystal structures of proteins (*47*). The tendency of αTS(1−188) to self-associate is also consistent with exposed hydrophobic surfaces in the F state. Parallel six-stranded open β sheet structures have been observed in more complex protein structures, which contain additional helices, loops, or subdomains that dock against the exposed side(s) of the sheet and prevent aggregation (*48*).

Further insight into the properties of the F state of αTS-(1−188) can be obtained by examining the unfolding kinetics of the fragment. A significant fraction of the equilibrium F state unfolds within 5 ms, revealing the presence of two kinetically distinct folded states, F′ and F″. The kinetically detected state with I1-like properties, F′, has a comparable stability and a slightly reduced *m* value to that measured for the equilibrium F state, suggesting that the free energy difference between these two principal folded states, F′ and F″, is small. The presence of a second folded state also explains the sensitivity of the native baselines to denaturant in the absorbance, circular dichroism, and fluorescence equilibrium titrations. Between 0 and 2 M urea, all three techniques show linear decreases in signal that are significantly greater than those observed for the native conformation of the full-length protein (*23, 30*). The absence of a sigmoidal change in signal in this region rules out a highly cooperative transition between the F′ and F″ states. Instead, simulations of the combined equilibrium and kinetic CD data to a three-state equilibrium model suggest that small differences in the optical properties of these two states and a small dependence of the relative populations on the denaturant concentration are sufficient to explain the behavior in the native baseline.

The absence of a change in the fluorescence anisotropy in the native baseline region (Figure 3) suggests that, unlike the secondary structure or exposure of tyrosines to solvent (Figure 2), the packing of several buried tyrosine side chains

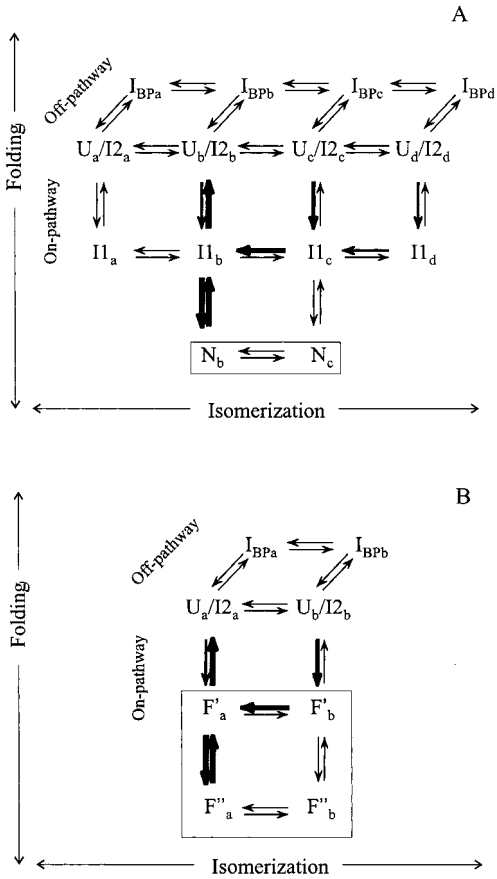

FIGURE 8: Proposed folding mechanism for full-length αTS (A) (*30*) and αTS(1−188) (B). The thicker arrows indicate the predominant folding/unfolding pathways. The species shown inside the boxes are observed at equilibrium in the absence of denaturant.

is similar in the F′ and F″ states. This peculiar behavior may reflect the dominant contributions of Y4, Y102, Y173, and Y175 that participate in the core of the β barrel and might be expected to be protected from solvent quenching. Tyrosine 169, located in a loop on the surface of full-length αTS, and tyrosine 115, positioned between two helices on the exterior of the barrel, may be sufficiently mobile in all members of the F thermodynamic state ensemble for the fragment that they would contribute little to the change in anisotropy induced by urea.

Kinetic Folding Properties of αTS(1−188). The folding of the full-length αTS protein has been previously demonstrated to involve multiple unfolded, intermediate, and native forms which fold through four parallel channels (Figure 8A) (*30*). Refolding initially proceeds through a set of off-pathway burst phase intermediates with significant secondary structure but marginal stability, $I_{BPa}-I_{BPd}$, which are populated within the dead-time of mixing (5 ms). Over the next several hundred milliseconds, the appearance of an on-pathway set of intermediates, $I1_a-I1_d$, which correspond to the equilibrium intermediate populated at 3 M urea, is limited by the unfolding of these burst phase intermediates. Only a minor population of the I1 intermediates, represented by $I1_b$, can fold directly to the native protein. Three slow (≥10 s) isomerization reactions play a critical role in controlling the folding of the majority of unfolded protein. The presence of these parallel folding channels has been suggested to involve the cis/trans isomerization about Xaa−Pro peptide bonds (*30*).

αTS(1−188) preserves several of the kinetic features observed for the full-length protein, including a significant burst phase in refolding and pairs of both unfolding and refolding reactions with time constants and urea dependences that are very similar to the two fastest detectable reactions (Figure 6). A folding mechanism for this fragment, based upon the mechanism for the full-length protein, can be proposed that accounts for the observed data (Figure 8B). Within 5 ms, two slowly interconverting unfolded forms, U_a (minor form) and U_b (major form), collapse to a corresponding pair of off-pathway intermediates, I_{BPa} and I_{BPb}, that are rich in secondary structure but have marginal stability. These burst phase intermediates then unfold over the next several hundred milliseconds to populate a pair of I1-like folded forms, F'_a and F'_b. The major folded form F'_b then undergoes a rate-limiting isomerization reaction to produce F'_a which in turn further folds to F''_a. The two unfolding phases reflect the independent unfolding of the major, F''_a, and minor, F''_b, forms that are presumed to unfold more rapidly than they interconvert. The F'_a and F'_b conformers unfold in the burst phase, similar to the I1 intermediate in full-length αTS.

The folding model for αTS(1−188) differs from that for the full-length protein in two significant ways. First, the I1-like species, F'_a and F'_b, are populated in the absence of denaturant, unlike the corresponding set for the full-length protein, $I1_a-I1_d$. Although the available data do not permit an accurate assessment of the relative populations of the F′ and F″ species, the relative amplitudes of the burst phase and subsequent slow unfolding phases (Figure 7) suggest that the relative populations of F′ and F″ are approximately 70% and 30%, respectively. Second, the observation of a single isomerization reaction for the refolding of the fragment implies that two of the four parallel channels (channels a and d) are absent. Given the tentative assignment of the three isomerization steps in αTS to a pair of proline isomerizations (*30*), it appears that one of these reactions may reflect the behavior of one of the six prolines in the 189−268 segment. Alternatively, it is possible that a proline residue contained in the αTS(1−188) fragment could be responsible for the loss of the slowest folding phases, particularly if the implicated proline residue interacts with residues in the C-terminal portion of the protein. Pro21, which is located in β strand 1, is a potential candidate because it makes contacts with residues in β strand 8. Mutagenic studies will ultimately be required to identify the role of specific prolines in the folding reaction of αTS.

A common feature of both folding models is the proposal of major and minor native conformers that unfold through parallel channels. The fact that Pro28, the only proline involved in a cis peptide bond, is contained in both polypeptides provides a possible explanation. The amplitude distribution of the two observable unfolding phases in αTS-(1−188) (93%/7%) as well as the absence of a direct refolding phase corresponding to the slowest unfolding phase in the fragment (Figure 6) is consistent with the dominant population of a trans proline in the unfolded form that is destined to adopt the cis isomer in the F state. Although replacement of Pro28 with Ala did not eliminate the slow folding reaction in the guanidine hydrochloride-induced unfolding of αTS (*29*), it is possible that a non-proline slow

isomerization is retained by a cis peptide bond in the mutant (*49*−*52*).

Utility of the Fragmentation Approach. The fragmentation approach has provided insights into the folding of full-length αTS by simplification of the folding mechanism. The loss of a pair of isomerization reactions in the refolding of the fragment implicates the carboxy-terminal segment, residues 189−268, as the source of these reactions. Also, the retention of the burst phase folding reaction, the 10 s isomerization reaction, and the pair of slow unfolding reactions show that most of the kinetic properties of the full-length protein are determined by residues 1−188. Thus, to a surprising extent for a single domain protein, the kinetic folding properties of αTS can be partitioned along with its sequence.

αTS(1−188) provides access to folding intermediates in the full-length protein by partially arresting folding at a particular point along the pathway. The major pair of folded forms of the fragment, F'_a and F'_b, are spectroscopically and thermodynamically similar to the I1 intermediate in full-length αTS. However, these I1-like species are not uniquely populated, but rather are in equilibrium with an additional pair of folded forms, F''_a and F''_b. This complex response demonstrates that comparisons of the folding mechanisms of fragments and full-length proteins must be done with care. In the case of αTS(1−188), the final product of the folding reaction appears to be a pair of non-native six-stranded conformations, F''_a and F''_b (*24*), which are avoided in the full-length protein by interaction with the two carboxy-terminal β strands.

General Implications for the Folding of TIM Barrels. The current study has demonstrated that a large fragment of a single domain protein can undergo a cooperative folding transition and retain a substantial portion of the folding mechanism of the full-length protein. These results are in contrast to fragments of other smaller single domain proteins, including chymotrypsin (*4*), barnase (*3*), and thioredoxin (*5*), which do not fold significantly. In the case of the TIM barrel motif, however, the sequential arrangement of the β strands preserves the majority of the nonlocal contacts in fragments. Previous equilibrium studies on a series of amino-terminal fragments of αTS have demonstrated that $\beta\alpha\beta$ modules make discrete contributions to their stabilities (*24*), suggesting that folding may involve the modular assembly of $\beta\alpha\beta$ super-secondary structure elements. The presence of both on- and off-pathway kinetic intermediates observed in the folding of αTS(1−188) presumably reflects the association of the remaining $\beta\alpha\beta$ modules either in cooperative, nativelike or in noncooperative, non-nativelike complexes, respectively. These diverse responses suggest that the subdomain (*1*) model should be expanded to include alternative higher-order structures whose appearance early in folding can retard the formation of the native conformation.

ACKNOWLEDGMENT

We thank Drs. O. Bilsel, K. E. Bowers, J. T. J. Lecomte, and V. F. Smith for helpful discussions.

REFERENCES

1. Oas, T. G., and Kim, P. S. (1988) *Nature 336*, 42−48.
2. Lecomte, J. T. J., and Matthews, C. R. (1993) *Protein Eng. 6*, 1−10.
3. Kippen, A. D., Sancho, J., and Fersht, A. R. (1994) *Biochemistry 33*, 3778−3786.
4. de Prat Gay, G., Ruiz-Sanz, J., Neira, J. L., Itzhaki, L. S., and Fersht, A. R. (1995) *Proc. Natl. Acad. Sci. U.S.A. 92*, 3683−3686.
5. Chaffotte, A. F., Li, J.-H., Georgescu, R. E., Goldberg, M. E., and Tasayco, M. L. (1997) *Biochemistry 36*, 16040−16048.
6. de Prat-Gay, G. (1996) *Protein Eng. 9*, 843−847.
7. Chaffotte, A. F., Cadieux, C., Guillou, Y., and Goldberg, M. E. (1992) *Biochemistry 31*, 4303−4308.
8. Gegg, C. V., Bowers, K. E., and Matthews, C. R. (1997) *Protein Sci. 6*, 1885−1892.
9. Jennings, P. A., Finn, B. E., Jones, B. E., and Matthews, C. R. (1993) *Biochemistry 32*, 3783−3789.
10. Missiakas, D., Betton, J.-M., Chaffotte, A., Minard, P., and Yon, J. M. (1992) *Protein Sci. 1*, 1485−1493.
11. Pecorari, F., Guilbert, C., Minard, P., Desmadril, M., and Yon, J. M. (1996) *Biochemistry 35*, 3465−3476.
12. Mann, C. J., Shao, X., and Matthews, C. R. (1995) *Biochemistry 34*, 14573−14580.
13. Gloss, L. M., and Matthews, C. R. (1998) *Biochemistry 37*, 15990−15999.
14. Miller, S., Schuler, B., and Seckler, R. (1998) *Biochemistry 37*, 9160−9168.
15. Speed, M. A., Wang, D. I., and King, J. (1995) *Protein Sci. 4*, 900−908.
16. Higgins, W., Fairwell, T., and Miles, E. W. (1979) *Biochemistry 18*, 4827−4835.
17. Miles, E. W., Yutani, K., and Ogasahara, K. (1982) *Biochemistry 21*, 2586−2592.
18. Beasty, A. M., and Matthews, C. R. (1985) *Biochemistry 24*, 3547−3553.
19. Tsuji, T., Chrunyk, B. A., Chen, X., and Matthews, C. R. (1993) *Biochemistry 32*, 5566−5575.
20. Ogasahara, K., Matsuhita, E., and Yutani, K. (1993) *J. Mol. Biol. 234*, 1197−1206.
21. Bilsel, O., Yang, L., Zitzewitz, J. A., Beechem, J. M., and Matthews, C. R. (1999) *Biochemistry 38*, 4177−4187.
22. Saab-Rincon, G., Froebe, C. L., and Matthews, C. R. (1993) *Biochemistry 32*, 13981−13990.
23. Gualfetti, P. J., Bilsel, O., and Matthews, C. R. (1999) *Protein Sci.* (in press).
24. Zitzewitz, J. A., Gualfetti, P. J., Perkons, I. E., Wasta, S. A., and Matthews, C. R. (1999) *Protein Sci. 8*, 1200−1209.
25. Hurle, M. R., and Matthews, C. R. (1987) *Biochim. Biophys. Acta 913*, 179−184.
26. Hurle, M. R., Michelotti, G. A., Crisanti, M. M., and Matthews, C. R. (1987) *Proteins: Struct., Funct., Genet. 2*, 54−63.
27. Tweedy, N. B., Hurle, M. R., Chrunyk, B. A., and Matthews, C. R. (1990) *Biochemistry 29*, 1539−1545.
28. Ogasahara, K., and Yutani, K. (1994) *J. Mol. Biol. 236*, 1227−1240.
29. Ogasahara, K., and Yutani, K. (1997) *Biochemistry 36*, 932−940.
30. Bilsel, O., Zitzewitz, J. A., Bowers, K. E., and Matthews, C. R. (1999) *Biochemistry 38*, 1018−1029.
31. Gill, S., and von Hippel, P. (1989) *Anal. Biochem. 182*, 319−326.
32. Shao, X., Hensley, P., and Matthews, C. R. (1997) *Biochemistry 36*, 9941−9949.
33. Pace, C. N., Shirley, B. A., and Thomson, J. A. (1990) in *Protein structure: A practical approach* (Creighton, T. E., Ed.) pp 311−330, IRL Press, Oxford.
34. Shao, X., and Matthews, C. R. (1998) *Biochemistry 37*, 7850−7858.
35. Mann, C. J., and Matthews, C. R. (1993) *Biochemistry 32*, 5282−5290.
36. Schellman, J. A. (1978) *Biopolymers 17*, 1305−1322.
37. Zitzewitz, J. A., Bilsel, O., Luo, J., Jones, B. E., and Matthews, C. R. (1995) *Biochemistry 34*, 12812−12819.
38. Slavik, J. (1982) *Biochim. Biophys. Acta 694*, 1−25.
39. Ptitsyn, O. B., Pain, R. H., Semisotnov, G. V., Zerovnik, E., and Razgulyaev, O. I. (1990) *FEBS Lett. 262*, 20−24.

40. Semisotnov, G. V., Rodionova, N. A., Razyguyaev, O. I., Oversky, V. N., Gripas, A. F., and Gilmanshin, R. I. (1991) *Biopolymers 31*, 119−128.
41. Engelhard, M., and Evans, P. A. (1995) *Protein Sci. 4*, 1553−1562.
42. Matthews, C. R. (1987) *Methods Enzymol. 154*, 498−511.
43. Kuwajima, K., Garvey, E. P., Finn, B. E., Matthews, C. R., and Sugai, S. (1991) *Biochemistry 30*, 7693−7703.
44. Raschke, T. M., and Marqusee, S. (1997) *Nat. Struct. Biol. 4*, 298−304.
45. Kuwajima, K., Garvey, E. P., Finn, B. E., Matthews, C. R., and Sugai, S. (1991) *Biochemistry 30*, 7693−7703.
46. Myers, J. K., Pace, C. N., and Scholtz, J. M. (1995) *Protein Sci. 4*, 2138−2148.
47. Lesk, A. M., Branden, C.-I., and Chothia, C. (1989) *Proteins: Struct., Funct., Genet. 5*, 139−148.
48. Branden, C., and Tooze, J. (1999) in *Introduction to Protein Structure*, p 410, Garland, New York.
49. Mayr, L. M., Willbold, D., Rosch, P., and Schmid, F. X. (1994) *J. Mol. Biol. 240*, 288−293.
50. Dodge, R. W., and Scheraga, H. A. (1996) *Biochemistry 35*, 1548−1559.
51. Jabs, A., Weiss, M. S., and Hilgenfeld, R. (1999) *J. Mol. Biol. 286*, 291−304.
52. Birolo, L., Malashkevich, V. N., Capitani, G., De Luca, F., Moretta, A., Jansonius, J., N., and Marino, G. (1999) *Biochemistry 38*, 905−913.
53. Hyde, C. C., Padlan, S. A., Miles, E. W., and Davies, D. R. (1988) *J. Biol. Chem. 263*, 17857−17871.
54. Kraulis, P. J. (1991) *J. Appl. Crystallogr. 24*, 946−950.
55. Nichols, B. P., and Yanofsky, C. (1979) *Proc. Natl. Acad. Sci. U.S.A. 76*, 5244.
56. Santoro, M. M., and Bolen, D. W. (1988) *Biochemistry 27*, 8063−8068.

BI9909041